Three-dimensional ray tracing of fast magnetosonic waves

Fuliang Xiao,[1,2] Qinghua Zhou,[1] Zhaoguo He,[1] and Lijun Tang[1]

Received 1 February 2012; revised 2 May 2012; accepted 3 May 2012; published 7 June 2012.

[1] A three dimensional ray tracing of fast magnetosonic (MS) waves is first performed by using a global core density model and a field-aligned density model. Simulating results show that MS waves are primarily confined within a few degrees of the geomagnetic equator due to magnetospheric reflection. MS waves originating from different *L*-shells on the dayside can propagate either into or out of the plasmasphere through the plasmapause. In particular, MS waves can propagate eastward (later MLT) or westward (earlier MLT) over a broad region of MLT. The current results further reveal a variety of propagation characteristics, particularly important for the MLT distribution of MS waves.

Citation: Xiao, F., Q. Zhou, Z. He, and L. Tang (2012), Three-dimensional ray tracing of fast magnetosonic waves, *J. Geophys. Res.*, *117*, A06208, doi:10.1029/2012JA017589.

1. Introduction

[2] Fast magnetosonic (MS) waves or equatorial noise are present as a series of narrow tones, spaced at multiples of the proton gyrofrequency f_{H^+} up to the lower hybrid resonance frequency f_{LH} [*Perraut et al.*, 1982]. Such MS waves are primarily confined within few degrees of the geomagnetic equator [*Russell et al.*, 1970; *Santolík et al.*, 2002; *Němec et al.*, 2005] and can propagate both inside and outside the plasmapause at very oblique wave normal angles.

[3] It has proposed that MS waves are generated by a ring distribution of ~10 keV energetic protons at frequencies close to the harmonics of the proton gyrofrequency [*Curtis and Wu*, 1979; *Gary et al.*, 2010]. The generation mechanism by proton rings is further confirmed by a recent survey of wave and particle data from the Satellite CRRES [*Meredith et al.*, 2008]. Equatorial MS waves can be very effective in accelerating electrons up to relativistic energies in the outer radiation belt via electron Landau resonance [*Horne et al.*, 2007] during active periods. The acceleration timescale can approach 1–2 days for the strongest MS waves, comparable to that due to whistler mode chorus waves [*Horne et al.*, 2005; *Li et al.*, 2007]. Moreover, a test particle simulation [*Bortnik and Thorne*, 2010] has demonstrated that MS waves can yield nonresonant transit time scattering of outer radiation belt energetic electrons because of the equatorial spatial confinement.

[4] Previous ray tracing calculations have been performed on the propagation characteristics and instability of MS waves over different frequencies [*Boardsen et al.*, 1992; *Horne et al.*, 2000]. Recently, some progresses have been made on understanding of the MLT distribution of MS waves and proton source. *Meredith et al.* [2008] have shown that strong MS waves can occur both inside the duskside plasmasphere and outside the plasmasphere mainly between 15:00–22:00 MLT and 01:00–04:00 MLT. These results suggest that MS waves can either be generated inside the plasmasphere, or propagate from outside to inside the plasmasphere at dusk. By incorporating the Rice Convection Model and the Ring Current-Atmospheric Interactions Model [*Jordanova et al.*, 2010; *Chen et al.*, 2010a], *Chen et al.* [2010b] have carried out a global analysis of the MS wave instability based on energetic proton phase space density during a geomagnetic storm. They have showed that the MS wave instability occurs at the local Alfven speed comparable to the proton ring velocity, and the unstable frequency band can be modulated by the ratio of the ring velocity and the local Alfven speed. They also find that lower frequency (<10 f_{H^+}) MS waves occur preferably in the high-density nightside plasmasphere and within the duskside plume, whereas higher frequency (>20 f_{H^+}) waves are present over a broad spatial region of low density outside the morningside plasmasphere. Moreover, simulations from LANL MPA data [*Chen et al.*, 2011] have demonstrated that MS wave instability at geosynchronous orbit occurs over a broad range of wave frequency from ~5 to 35 f_{H^+} and over a broad MLT range from 1000 to 2200, where the proton ring distributions are preferentially observed. Interestingly, there exists different MTL distribution of observed proton source and MS waves. Such discrepancy occurs probably due to the azimuthal propagation from near noon toward dawn. However, there has been no systematic analysis of how MS waves propagate in MLT and through the plasmapause. Consequently, a three-dimensional (3D) ray tracing study is required to examine the importance of off-meridian propagation.

2. 3D Ray Tracing

[5] Analogous to the previous works [*Horne*, 1989; *Chen et al.*, 2010b], we define the following local Cartesian

[1]School of Physics and Electronic Sciences, Changsha University of Science and Technology, Changsha, China.
[2]State Key Laboratory of Space Weather, Chinese Academy of Sciences, Beijing, China.

Corresponding author: F. Xiao, School of Physics and Electronic Sciences, Changsha University of Science and Technology, Changsha 410004, China. (flxiao@126.com)

0148-0227/12/2012JA017589

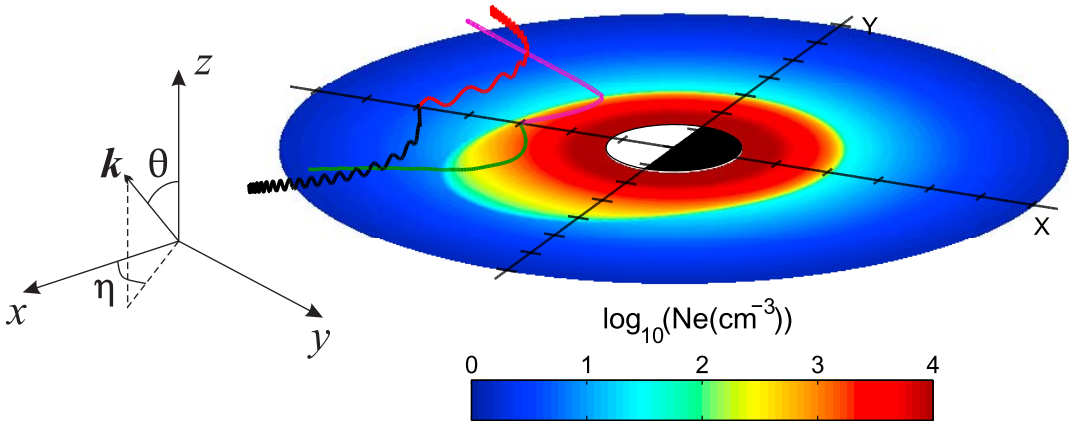

Figure 1. (left) Geometry of wave vector k in a local coordinate system with z axis along the direction of the ambient magnetic field. (right) A three dimensional view of the raypaths of magnetosonic waves with $f = 38$ Hz, $\theta_0 = 89.5°$, $\eta_0 = 120°$ (black and green lines) and 240° (red and magenta lines), launched at the equator at MLT = 12, $L = 3$ and 5 (shown). The background equatorial density is superimposed in color scale.

system for 3D ray tracing (see Figure 1). In such local Cartesian system, the z axis points along the direction of the ambient magnetic field, the x axis is orthogonal to the z axis and stays in the meridian plane pointing away from the Earth at the equator, and the y axis completes the right-handed set. The wave vector **k** makes an angle θ with the z axis and the projection of **k** onto the xy plane makes an angle η with the x axis. $\eta = 0°$, 90°, 180° and 270° correspond to the perpendicular component $\mathbf{k}_\perp$ pointing away from the Earth, toward later MLT (eastward), toward the Earth, and toward earlier MLT (westward), respectively.

[6] In this study we adopt a recently developed program [*Xiao et al.*, 2007] which is based on the methodology of the HOTRAY code [*Horne*, 1989]. We focus on the high geomagnetic activity ($K_p = 6$), and adopt a dipole magnetic field model together with a plasma density model which combines the global core plasma model [*Gallagher et al.*, 2000] and the field-aligned density variation model [*Denton et al.*, 2002]. Considering that the rays launched outward basically propagate straight outward, and such outward propagation analysis has been made in detail by *Horne et al.* [2000], in order for a more thorough investigation on the propagation characteristics, in the following we choose all the raypaths to be launched toward the Earth, i.e., $90° \le \eta_0 \le 270°$.

[7] Figure 1 shows an example of 3D raypaths of fast MS waves launched at the equator at MLT = 12, $L = 3$ and 5, with wave frequency $f = 38$ Hz, initial $\theta_0 = 89.5°$, $\eta_0 = 120°$ and 240°. Propagation characteristics of those raypaths are also shown in Figure 2. The rays inside the plasmasphere ($L = 3$) pass gradually through the plasmapause and propagate outside the plasmasphere eastward (later MLT) for initial $\eta_0 = 120°$ and westward (earlier MLT) for initial $\eta_0 = 240°$. The rays outside the plasmasphere ($L = 5$) propagate outside the plasmasphere toward either later MLT (eastward) for initial $\eta_0 = 120°$ or earlier MLT (westward) for initial $\eta_0 = 240°$. All the four rays are confined within a few degrees of equator due to magnetospheric reflection (Figure 2a). Magnetospheric reflection occurs at which the wave reverses the component of its group velocity along the ambient magnetic field. Moreover, such four rays propagate

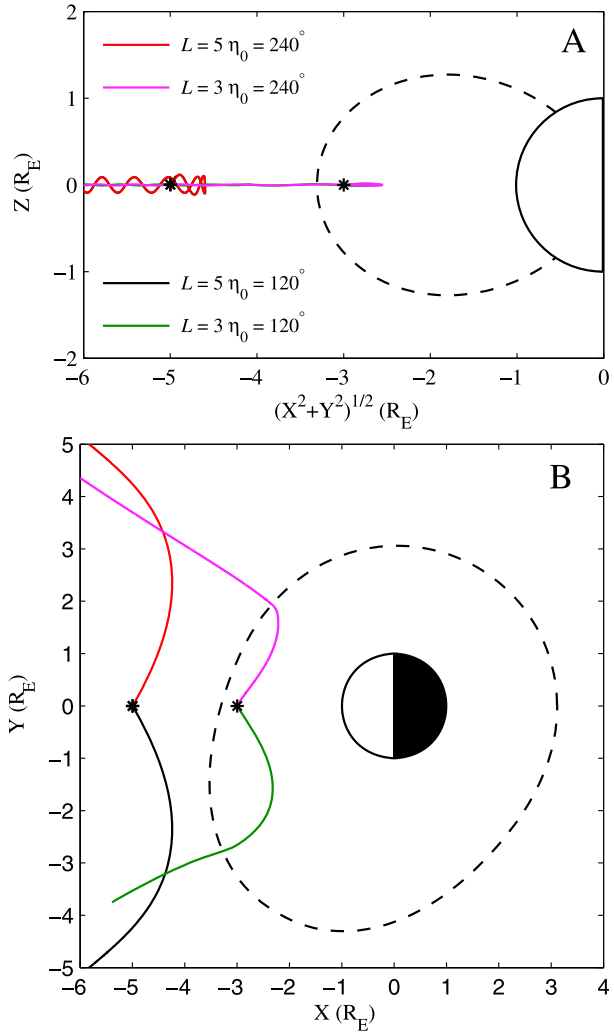

Figure 2. Corresponding to Figure 1, the projections of raypaths on the (a) R_{XY}-Z plane and (b) X-Y plane with different launching positions (asterisks). The dashed line corresponds to the plasmapause position at MLT = 12 (top) and at the equator (bottom).

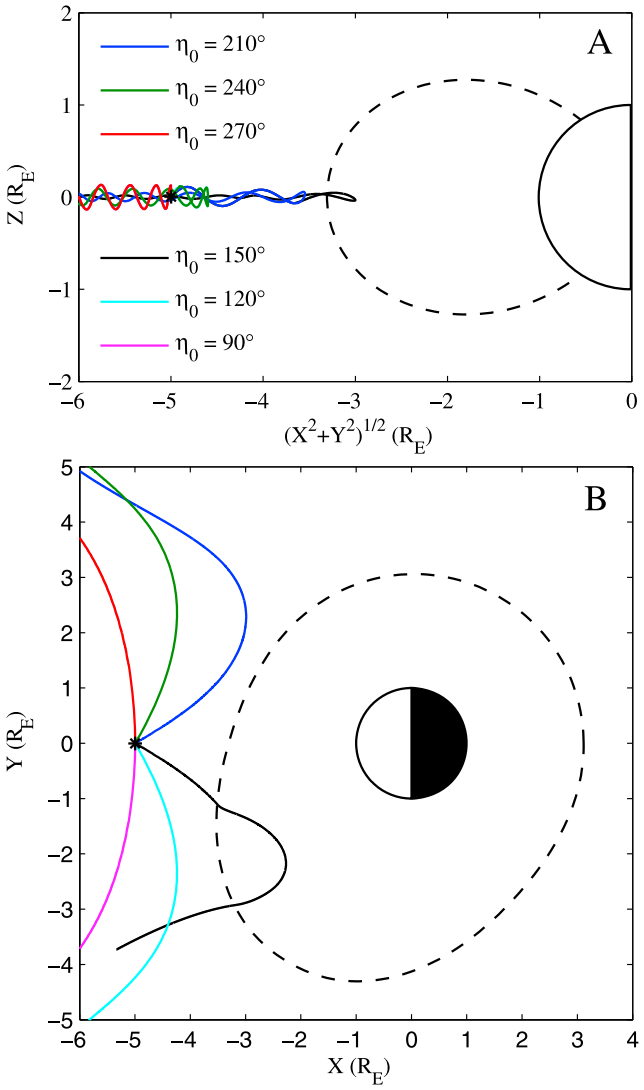

Figure 3. The projections of raypaths of the magnetosonic waves for different initial azimuthal angles (shown), launched at L = 5 and MLT = 12, with f = 38 Hz, θ_0 = 89.5°. The dashed lines corresponds to the plasmapause position.

toward lower L-shell at first due to launching direction toward the Earth and then gradually turn back toward high L-shells due to approaching the higher density region (Figure 2b). The major reason is that the refraction index basically decreases as density increases. According to Snell's law, the angle between the wave group velocity and the density gradient (the normal to the density surface) increases as density increases. Thus the ray turns back when the wave approaches higher density region.

[8] Figure 3 shows the propagation characteristics of rays for different initial azimuthal angles launched at L = 5 and MLT = 12, with f = 38 Hz, θ_0 = 89.5°. Similarly, all the ray trajectories stay near the equator, propagate toward lower L-shell at first and then turn back toward high L-shells. In particular, the raypath with η_0 = 150° propagates inside the plasmasphere at first and then travels outside by crossing the plasmapause twice. As mentioned above, the angle between the wave group velocity and the density gradient increases as density increases. If the density variation across the plasmapause increases sharply, the angle between both can increase to 90 or above, and then drive the ray back without penetrating into the plasmasphere. Hence, the criterion for the plasmapause crossing is a gradual density variation across the plasmapause, like near the plume around duskside. This result give a possible explanation for the observation of intensified MS waves both inside the duskside plasmasphere and outside the plasmasphere mainly between 15:00–22:00 MLT [*Meredith et al.*, 2008]. Figure 4 plots the ray trajectories with the same parameters as those in Figure 3 but for L = 3 (inside the plasmasphere) and f = 176 Hz. Clearly, all the rays stay close to the equator and propagate out of the plasmasphere through the plasmapause toward higher L-shells.

[9] Figure 5 presents the projections of raypaths launched at L = 5 and MLT = 12, with different wave frequencies (shown), θ_0 = 89.5°, η_0 = 120° and 240°. When wave

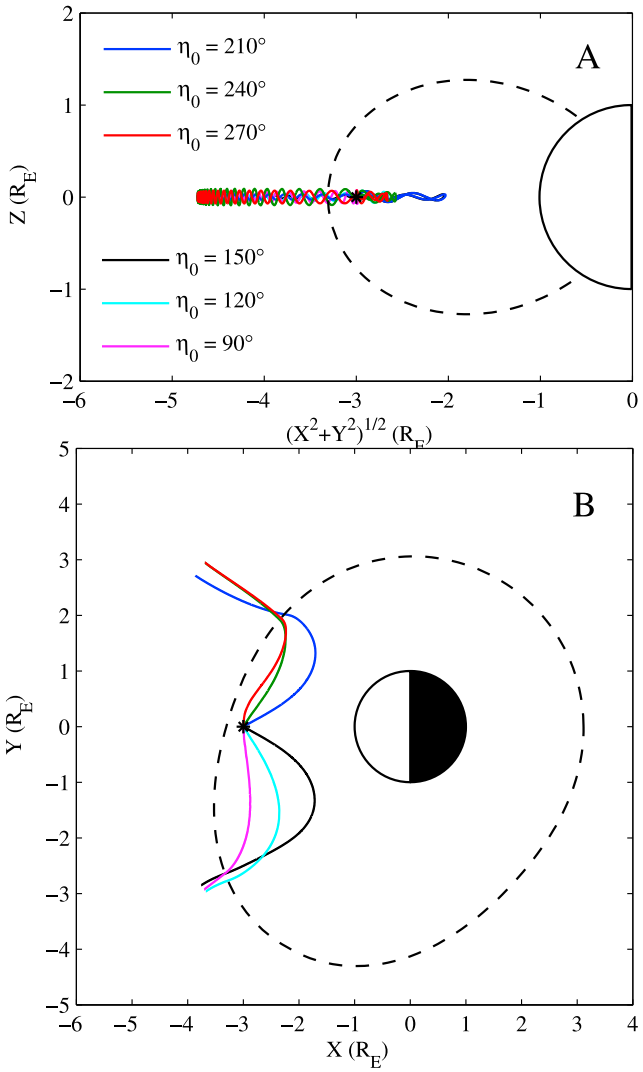

Figure 4. Same as Figure 3 but for L = 3 and f = 176 Hz or 10 f_{H+}, here f_{H+} is local equatorial gyrofrequency of hydrogen.

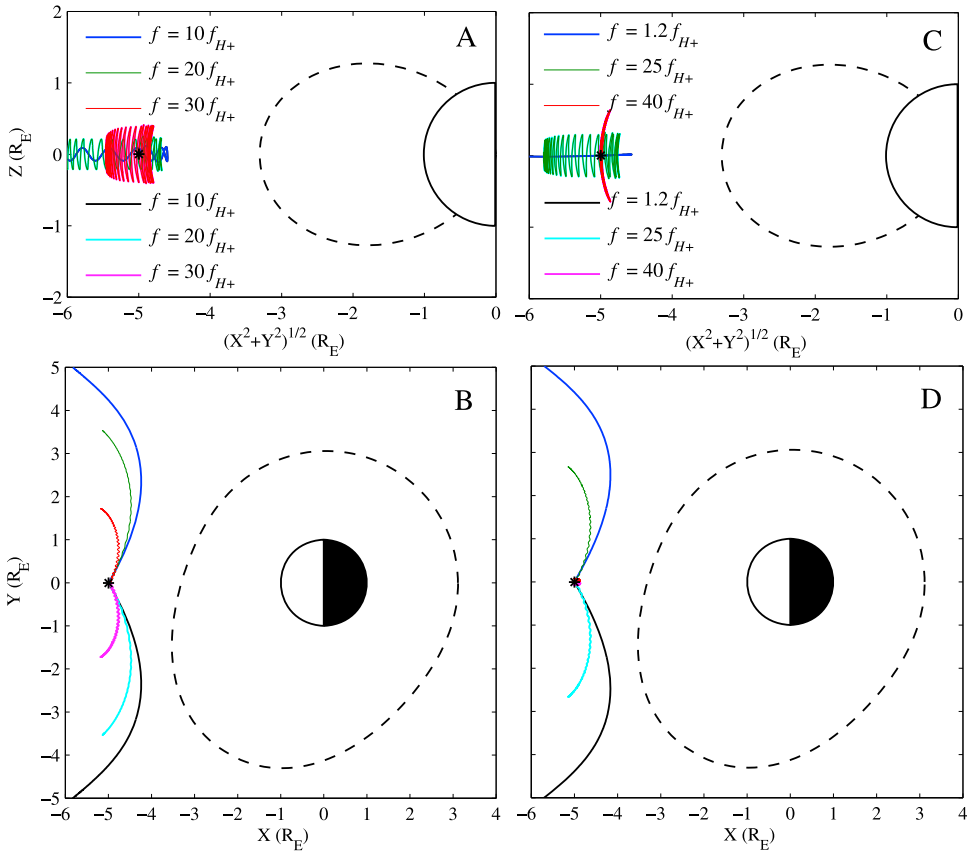

Figure 5. (a–d) The projections of raypaths of magnetosonic waves launched at L = 5 and MLT = 12, with different wave frequencies (shown), θ_0 = 89.5°, η_0 = 120° and 240°.

frequency decreases from 40 f_{H^+} (~0.99 f_{LH}) to 1.2 f_{H^+}, the raypath moves toward a lower latitude (Figures 5a and 5c) but over a broader range of MLT and L-shell (Figures 5b and 5d). In particular, the raypath is confined near the equator for frequency close to the proton gyrofrequency (Figure 5c), a behavior different from that of typical EMIC waves. Whereas, the raypath stays near the source MLT and L-shell for frequency close to the lower hybrid frequency (Figure 5d), which is different from typical whistler mode waves. Those different propagation characteristics of MS waves from EMIC or whistler mode waves shall yield different role of MS waves on radiation belt dynamics. As analyzed in detail by *Boardsen et al.* [1992], this is primarily because the wave with a lower frequency has a higher perpendicular component (correspondingly a lower parallel component) of group velocity than that with a higher frequency as the wave normal angle close to 90°. Since magnetospheric reflection occurs at the reversion of the parallel component of group velocity, the parallel component magnitude basically determines the maximum wave propagation latitude. Meanwhile, the perpendicular component magnitude roughly controls the wave propagation range of MLT and L-shell. Consequently, the lower frequency wave encounters magnetospheric reflection at lower latitude but travels over a broader range of MLT and L-shell at a given ray tracing time.

[10] Raypaths starting at different L-shells are plotted in Figure 6 for MLT = 14, f = 38 Hz, θ_0 = 89.5°, η_0 = 120° and 240°. Obviously, the raypaths launched inside (L = 3) and outside (L = 5) the plasmasphere exhibit the analogous features to those in Figure 2. The two raypaths launched at the plasmapause (L = 4) propagate toward lower L-shells inside the plasmasphere at first, even very deep inward for η_0 = 240°. Then both rays turns back toward higher L-shells when they encounter the higher density region, propagate both eastward (later MLT) across the plasmapause though the initial **k** pointing westward for η_0 = 240°, probably due to the asymmetry of the plasmasphere shape during storm conditions.

[11] To examine the effect of different initial wave normal angles on ray trajectories, we present ray tracing results in Figure 7 by choosing three angles: θ_0 = 89.5°, 85° and 80°. We don't consider the cases below 80° since a huge Landau damping limits the length of the raypath for wave normal angle θ_0 < 85° [*Horne et al.*, 2000]. As shown in Figure 7, the raypath for 80° can travel to higher latitude than that for 89.5° or 85°, consistent with the previous result that a smaller normal angle wave encounters reflection at higher geomagnetic latitudes [*Boardsen et al.*, 1992]. The major reason is that a smaller normal angle wave basically has a larger parallel component of group velocity, yielding propagation toward higher latitude.

[12] It should be noted that we do not take into account of Landau damping in the current calculation. *Horne et al.* [2000] have shown that electron Landau resonant energy E_{res} basically decreases with decreasing wave normal angles.

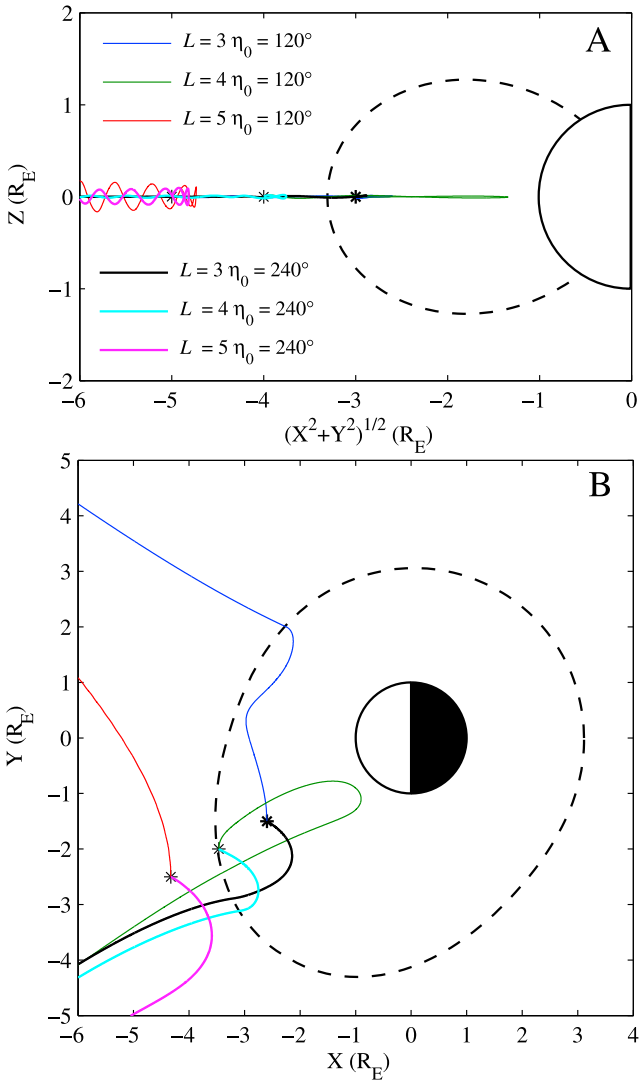

Figure 6. The projections of raypaths of magnetosonic waves launched at different L-shells (shown) at MLT = 14, with f = 38 Hz, θ_0 = 89.5°, η_0 = 120° and 240°.

For wave normal angle below 85°, E_{res} drops dramatically down to tens of eV, leading to a large Landau damping. Hence, electron Landau damping should limit propagation of MS waves to be almost perpendicular to the magnetic field and thus close to the equator.

3. Summary

[13] Adopting a global core density model and a field-aligned density model, we present a initial 3D ray tracing of fast magnetosonic waves. We focus on the high geomagnetic activity (K_p = 6) and choose all the raypaths to be launched toward the Earth. We find that MS waves are primarily confined within a few degrees of the geomagnetic equator due to magnetospheric reflection. The lower the wave frequency is, the closer it stays to the equator. This is because the wave with a smaller frequency has a smaller parallel component of group velocity than that with a higher frequency as the wave normal angle approaches 90°, yielding magnetospheric reflection at lower latitude for a lower wave frequency. Similarly, wave with a smaller normal angle can travel to higher latitude than that with a higher normal angle due to a larger parallel component of group velocity. Moreover, MS waves launched at different L-shells on the dayside can propagate either into or out of the plasmasphere through the plasmapause. Such plasmapause crossing occurs at a gradual density variation across the plasmapause, like near the plume around duskside, consistent with the observation. In particular, MS waves can propagate eastward (later MLT) or westward (earlier MLT) over a broad range of MLT, tempting to account for local time distribution differences of observed MS waves and proton source. Finally, since fast MS waves can be responsible for either local acceleration or transit time scattering of outer radiation belt electrons, the current results shall provide further knowledge on how MS waves influence radiation belt dynamics during active periods.

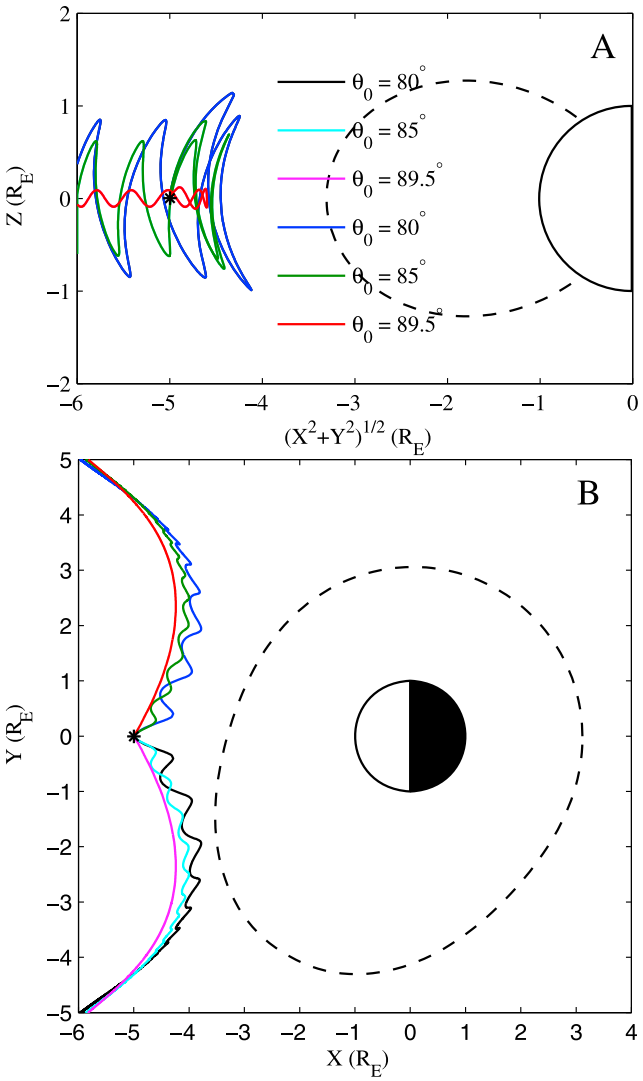

Figure 7. The projections of raypaths of magnetosonic waves launched at different initial wave normal angles (shown) at L = 5 and MLT =12, with f = 38 Hz, η_0 = 120° and 240°.

[14] **Acknowledgments.** This work is supported by 973 Program 2012CB825603, the National Natural Science Foundation of China grants 40931053, 40925014, the Specialized Research Fund for State Key Laboratories, and the construct program of the key discipline in Hunan Province.

[15] Robert Lysak thanks the reviewers for their assistance in evaluating this paper.

References

Boardsen, S. A., D. L. Gallagher, D. A. Gurnett, W. K. Peterson, and J. L. Green (1992), Funnel-shaped, low-frequency equatorial waves, *J. Geophys. Res.*, *97*(A10), 14,967–14,976, doi:10.1029/92JA00827.

Bortnik, J., and R. M. Thorne (2010), Transit time scattering of energetic electrons due to equatorially confined magnetosonic waves, *J. Geophys. Res.*, *115*, A07213, doi:10.1029/2010JA015283.

Chen, L., R. M. Thorne, V. K. Jordanova, C. Wang, M. Gkioulidou, L. Lyons, and R. B. Horne (2010a), Global simulation of EMIC wave excitation during the 21 April 2001 storm from coupled RCM-RAM-HOTRAY modeling, *J. Geophys. Res.*, *115*, A07209, doi:10.1029/2009JA015075.

Chen, L., R. M. Thorne, V. K. Jordanova, and R. B. Horne (2010b), Global simulation of magnetosonic waves instability in the storm time magnetosphere, *J. Geophys. Res.*, *115*, A11222, doi:10.1029/2010JA015707.

Chen, L., R. M. Thorne, V. K. Jordanova, M. F. Thomsen, and R. B. Horne (2011), Magnetosonic wave instability analysis for proton ring distributions observed by the LANL magnetospheric plasma analyzer, *J. Geophys. Res.*, *116*, A03223, doi:10.1029/2010JA016068.

Curtis, S. A., and C. S. Wu (1979), Gyroharmonic emissions induced by energetic ions in the equatorial plasmasphere, *J. Geophys. Res.*, *84*(A6), 2597–2607, doi:10.1029/JA084iA06p02597.

Denton, R. E., J. Goldstein, J. D. Menietti, and S. L. Young (2002), Magnetospheric electron density model inferred from Polar plasma wave data, *J. Geophys. Res.*, *107*(A11), 1386, doi:10.1029/2001JA009136.

Gallagher, D. L., P. D. Craven, and R. H. Comfort (2000), Global core plasma model, *J. Geophys. Res.*, *105*(A8), 18,819–18,833, doi:10.1029/1999JA000241.

Gary, S. P., K. Liu, D. Winske, and R. E. Denton (2010), Ion bernstein instability in the terrestrial magnetosphere: Linear dispersion theory, *J. Geophys. Res.*, *115*, A12209, doi:10.1029/2010JA015965.

Horne, R. B. (1989), Path-integrated growth of electrostatic waves: The generation of terrestrial myriametric radiation, *J. Geophys. Res.*, *94*(A7), 8895–8909, doi:10.1029/JA094iA07p08895.

Horne, R. B., G. V. Wheeler, and H. S. C. K. Alleyne (2000), Proton and electron heating by radially propagating fast magnetosonic waves, *J. Geophys. Res.*, *105*(A12), 27,597–27,610, doi:10.1029/2000JA000018.

Horne, R. B., R. M. Thorne, S. A. Glauert, J. M. Albert, N. P. Meredith, and R. R. Anderson (2005), Timescale for radiation belt electron acceleration by whistler mode chorus waves, *J. Geophys. Res.*, *110*, A03225, doi:10.1029/2004JA010811.

Horne, R. B., R. M. Thorne, S. A. Glauert, N. P. Meredith, D. Pokhotelov, and O. Santolík (2007), Electron acceleration in the Van Allen radiation belts by fast magnetosonic waves, *Geophys. Res. Lett.*, *34*, L17107, doi:10.1029/2007GL030267.

Jordanova, V. K., R. M. Thorne, W. Li, and Y. Miyoshi (2010), Excitation of whistler-mode chorus from global ring current simulations, *J. Geophys. Res.*, *115*, A00F10, doi:10.1029/2009JA014810.

Li, W., Y. Y. Shprits, and R. M. Thorne (2007), Dynamic evolution of energetic outer zone electrons due to wave-particle interactions during storms, *J. Geophys. Res.*, *112*, A10220, doi:10.1029/2007JA012368.

Meredith, N. P., R. B. Horne, and R. R. Anderson (2008), Survey of magnetosonic waves and proton ring distributions in the earth's inner magnetosphere, *J. Geophys. Res.*, *113*, A06213, doi:10.1029/2007JA012975.

Němec, F., O. Santolík, K. Gereová, E. Macúšová, Y. de Conchy, and N. Cornilleau-Wehrlin (2005), Initial results of a survey of equatorial noise emissions observed by the Cluster spacecraft, *Planet. Space Sci.*, *53*, 291–298, doi:10.1016/j.pss.2004.09.055.

Perraut, S., A. Roux, P. Robert, R. Gendrin, J. Sauvaud, J. Bosqued, G. Kremser, and A. Korth (1982), A systematic study of ULF waves above FH+ from GEOS 1 and 2 measurements and their relationships with proton ring distributions, *J. Geophys. Res.*, *87*(A8), 6219–6236, doi:10.1029/JA087iA08p06219.

Russell, C. T., R. E. Holzer, and E. J. Smith (1970), OGO 3 observations of ELF noise in the magnetosphere: 2. The nature of the equatorial noise, *J. Geophys. Res.*, *75*(4), 755–768, doi:10.1029/JA075i004p00755.

Santolík, O., J. S. Pickett, D. A. Gurnett, M. Maksimovic, and N. Cornilleau-Wehrlin (2002), Spatiotemporal variability and propagation of equatorial noise observed by cluster, *J. Geophys. Res.*, *107*(A12), 1495, doi:10.1029/2001JA009159.

Xiao, F., L. Chen, H. N. Zheng, and S. Wang (2007), A parametric ray tracing study of superluminous auroral kilometric radiation wave modes, *J. Geophys. Res.*, *112*, A10214, doi:10.1029/2006JA012178.